Estimation of Volatile Organic Compound Mass Transfer Coefficients in the Vacuum Desorption of Acetone from Activated Carbon

Liqing Li,* Zheng Liu, Yingxin Qin, Zheng Sun, Jianfei Song, and Lin Tang

School of Energy Science and Engineering, Central South University, Changsha 410083, China

The export concentrations of acetone desorption from activated carbon at different temperatures, vacuum degrees, and saturated adsorption capacities were measured. The results showed that the greater the desorption vacuum degree and the initial adsorption capacity, the smaller the desorption rate. Given the adsorbent microporous capillary effect and the mass transfer in the process of desorption, the concentration curve reflects three phases, which are the vacuum-concentrated phase, fast attenuation phase, and slow attenuation phase. Through theoretical analysis and a coupled model of the desorption process, numerical simulation of the acetone desorption from activated carbon was carried out. Experimental and theoretical analysis showed that small temperature changes were caused by desorption; therefore, the change of the mass transfer coefficient and concentration caused by the temperature change is also small. In different desorption phases, a coupled effect on the mass transfer coefficients have different influences on the concentration curve. For the same initial adsorption capacity, the greater the partial pressure of the acetone, the larger the mass transfer coefficient. Obtaining the mass transfer coefficient and axial dispersion coefficient by sections can make the numerical results coincide well with the experimental data, and the axial diffusion coefficient should not be ignored in vacuum desorption.

Introduction

In recent years, adsorption has become more widely applied in large-scale separation projects, such as the separation and recovery of organic solvents,[1,2] purification of sulfur dioxide, nitrogen oxides,[3] mercury vapor,[4] and dioxins[5] and other pollutants in combustion gas, carbon oxygen capture and storage,[6] and so on. PSA (pressure swing adsorption) is one of the most important applications. On the basis of the fact that adsorption varies under different pressures, it achieves the separation of gas and the recycling of sorbents.[1,7] It has been found in previous studies that the smaller the desorption vacuum degree, the steeper the desorption curve. However, when the export concentration decreases to half of the initial concentration, the desorption rate decreases considerably, and the export concentration curve is abnormal and does not follow the law of atmospheric pressure desorption. Additionally, the rebound and maintenance of the concentration is also abnormal, and this phenomenon is particularly evident with a total desorption pressure below 30 kPa. This phenomenon has to do with both the capillary effect and the heat and mass transfer cross-coupling effect.[8,9] At present, there are plenty of experimental studies and numerical simulations of the heat and mass transfer in the adsorption process,[10,11] while there is less research on desorption, particularly vacuum desorption.[2] Subebach[2] takes vacuum desorption as a counter-process of adsorption. However, in this research, it is proven that, under a larger vacuum degree, the export concentration for desorption and adsorption are not the opposite but rather are more complex. A heat and mass transfer coupling model was established for vacuum desorption to simulate the desorption process of acetone from the activated carbon. It serves as a numerical method of study on the coupled heat and mass transfer on the desorption and provides reference for the adsorption kinetic study of the purification of other pollutants.

* Corresponding author. Tel.: +86 073188877195. Fax: +86 073188879863. E-mail: liqingli@hotmail.com.

Experimental System and Methodology

Fixed-bed adsorption was used to study the desorption process. The device consists of gas distribution systems, a constant temperature system, an adsorption column (filled length $L = 0.4$ m, diameter $D_{Bi} = 0.028$ m), a test system (GC FID, RS53-T, Ratfisch nahysystem, Germany), data-processing systems (solatron instrument), and two vacuum pumps [(80 to 100) kPa]. The inlet concentration of organic gases is measured in the bypass pipe at the entrance of the adsorption column; the outlet concentration is measured at the exports of the adsorption column. Thermocouples are inside the adsorption column 1 cm away from the surface. These are used to measure the temperature changes in the heat and mass transfer areas as a result of released or absorbed heat by activated carbon absorption or desorption.

Columnar activated carbon C40/4 (Carbotech. Ltd. Co., Germany) was used in this study as the adsorbent, whose specific physical performance parameters are shown in Table 1; acetone (Koster and Bohmke Ltd., Germany) was used as absorbate, with a purity over 99.5 %. The experimental apparatus is shown in Figure 1.

Adsorption experiments were first done before desorption. The vacuum pump blows a certain concentration of dry organic gas (acetone) into the adsorption column of laminated glass with a constant internal water temperature to ensure a constant temperature in areas beyond the mass transfer regions. When the adsorption column outlet gas concentration equals that of the inlet gas for more than 30 min, dynamic balance is achieved. The mass of activated carbon is measured to determine the adsorption capacity and thereby determine the parameters in the adsorption isotherm model.

10.1021/je1003548
Published on Web 09/10/2010

Table 1. Parameters of Activated Carbon (C40/4)

bulk density	apparent density	BET[a] surface area		micropore volume	specific heat capacity	particle size
$kg \cdot m^{-3}$	$kg \cdot m^{-3}$	$m^2 \cdot kg^{-1}$	porosity	$m^3 \cdot kg^{-1}$	$kJ \cdot K^{-1} \cdot kg^{-1}$	($d \times L$)
390	700	106	0.667	10^{-3}	0.8	0.004 mm × 0.008 mm

[a] Brunauer−Emmett−Teller.

After weighing, the activated carbon is put back into adsorption column. Organic gases with the original inlet concentration go through the carbon for adsorption. After the adsorption balance is achieved, the adsorption vacuum pumps are replaced with the desorption vacuum pump. By adjusting the constant water temperature, inlet concentration, and desorption vacuum, we may obtain different export concentrations. When the adsorption column outlet gas concentration equals that of the intake for more than 30 min, desorption balance is achieved. At the same time, the activated carbon is weighed to determine the desorption capacity.

Mathematical Model

Assumptions. Several assumptions are made to build the model to analyze the test data and study the heat and mass transfer coupling in the adsorption column, and Athena was used to do the simulations in this work.

(1) The gas is viewed as an ideal gas (because when the gas is at low pressure and room temperature, the effect of pressure and temperature on the gas is neglected).

(2) The bed pressure drop is ignored (this work ignored the role of resistance).

(3) The linear driving force mass transfer model is used (a traditional model is used in this work).

(4) The adsorption equilibrium model uses the Langmuir adsorption isotherm model.

(5) The adsorption of the carrier gas is neglected (because activated carbon has little adsorption capacity for the carrier gas).

(6) Gases within the fixed bed are in the form of axial piston flow (because of little radical diffusion).

(7) The gas flows uniformly on every surface of the bed. Considering the constant adsorbate, the gas flow rate in the fixed bed is constant (to simplify the adsorption process).

(8) The physical properties of the adsorbents and the adsorption column do not change.

Model Development. Gas-Phase Mass Transfer Model. The model used in gas-phase mass transfer is

$$-D_L\frac{\partial^2 C}{\partial z^2} + u\frac{\partial C}{\partial z} + \frac{\partial C}{\partial t} + \frac{1-\varepsilon}{\varepsilon}\rho_p\frac{\partial q}{\partial t} = 0 \qquad (1)$$

where D_L is the axial diffusion coefficient, $m \cdot s^{-1}$; C is the total concentration of gas, $kg \cdot m^{-3}$; u is the empty tower gas velocity, $m \cdot s^{-1}$; ϵ is the adsorbent porosity; z is the bed axial coordinates; ρ_p is the adsorbent packing density, $kg \cdot m^{-3}$; q is the solid-phase concentration, $kg \cdot kg^{-1}$; and t is the adsorption time, s.

Adsorbed gases meet the ideal gas assumption, namely, $C_i = py_iM_i/(RT)$. C_i is a concentration of component i, $kg \cdot m^{-3}$; y_i is mole fraction of component i; M_i is molar mass of component i, $kg \cdot mol^{-1}$; R is the gas constant, $J \cdot (mol \cdot K)^{-1}$; T is the gas temperature in the column, K; and p is the column internal pressure, Pa.

These are introduced into eq 1, such that,

$$-D_L\frac{\partial^2 y_i}{\partial z^2} + u\frac{\partial y_i}{\partial z} + \frac{\partial y_i}{\partial t} + \frac{1-\varepsilon}{\varepsilon}\rho_p\frac{RT}{pM_i}\frac{\partial q}{\partial t} = 0 \qquad (2)$$

Energy Conservation Model. The model used for energy conservation is

$$-\varepsilon K_L\frac{\partial^2 T}{\partial z^2} + (\varepsilon_t\rho_g c_{pg} + \rho_B c_{ps} + \rho_B c_{pa} q)\frac{\partial T}{\partial t} + \varepsilon\rho_g c_{pg} u\frac{\partial T}{\partial z} + \rho_B\Delta H\frac{\partial q}{\partial t} + \frac{2a_w}{R_{Bi}}(T - T_w) = 0 \qquad (3)$$

where K_L is the thermal axial dispersion coefficient, $W \cdot (m^2 \cdot K)^{-1}$; c_{pg} is the column gas heat capacity, $J \cdot (mol \cdot K)^{-1}$; c_{ps} is the solid-phase adsorbent heat capacity, $J \cdot (kg \cdot K)^{-1}$; c_{pa} is the heat capacity of the absorbed phase, $J \cdot (mol \cdot K)^{-1}$; ρ_B is a true bed density, $kg \cdot m^{-3}$; ρ_g is the column gas density, $kg \cdot m^{-3}$; ΔH is the equivalent heat adsorption, $J \cdot mol^{-1}$; a_w is the effective heat transfer coefficient of the wall, $J \cdot (s \cdot K)^{-1}$; R_{Bi} is the bed internal radius, m; and T_w is the wall temperature, K.

The wall heat transfer in axial dispersion is neglected, and to calculate the bed boundary energy, the energy equation is

$$\rho_w c_{pw} A_w\frac{\partial T_w}{\partial t} - 2\pi R_{Bi} h_i(T - T_w) + 2\pi R_{Bo} h_o(T_w - T_{atm}) = 0 \qquad (4)$$

$$A_w = \pi({R_{Bo}}^2 - {R_{Bi}}^2)$$

ρ_w is the bed wall density, $kg \cdot m^{-3}$; c_{pw} is the bed wall heat capacity, $J \cdot (mol \cdot K)^{-1}$; A_w is the bed wall cross-sectional area, m^2; R_{Bo} is the bed wall external radius, m; h_i is the convective heat transfer coefficient, $J \cdot (s \cdot K)^{-1}$; h_o is the natural convection heat transfer coefficient; and T_{atm} is the ambient temperature, K.

Mass Transfer Rate Equation and Adsorption Isotherm Equation in the Linear Driving Force Mass Transfer Model (LDF). The LDF mass transfer rate equation is

$$\frac{\partial q}{\partial t} = k(q^* - q) \qquad (5)$$

where q^* is the equilibrium adsorption capacity, $kg \cdot kg^{-1}$.

The adsorption isotherm (Langmuir) equation is

$$q^* = q_{max}\frac{bC}{1 + bC} \qquad (6)$$

where q_{max} is the maximum adsorption capacity, $kg \cdot kg^{-1}$, and $q_{max} = aa \exp(bb/T)$, $b = cc \exp(dd/T)$.[8,12] aa, bb, cc, and dd are fitting constants, where $aa = 2.4279 \cdot 10^{-3}$, $bb = 1.4193 \cdot 10^3$, $cc = 2.0975 \cdot 10^{-4}$, and $dd = 1.9202 \cdot 10^3$, respectively.

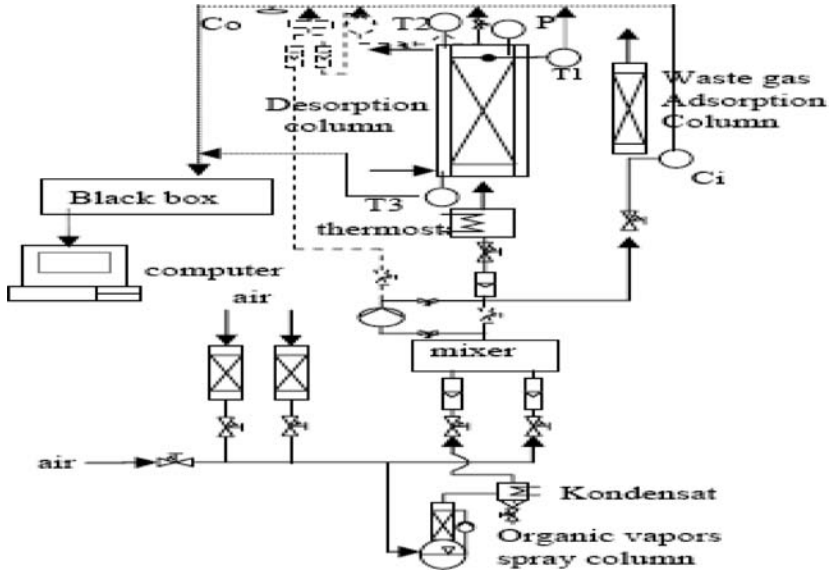

Figure 1. Experimental device.

Theoretically, the mass transfer coefficient[9,13] can be obtained by

$$k = \frac{15}{R_p^2} \cdot \frac{D_{eff}}{1 + \frac{\rho_S}{\varepsilon_p} \cdot \frac{\partial q}{\partial c}} \tag{7}$$

$$D_{eff} = 1/\left(\frac{1}{D'_{12}} + \frac{1}{D'_{kn}}\right) \tag{8}$$

$$D_{12} = \frac{0.00143T^{1.75}\left[\frac{M_1 + M_2}{M_1 M_2}\right]^{0.5}}{p[V_1^{1/3} + V_2^{1/3}]^2} \tag{9}$$

$$D_{kn} = \frac{4}{3} d_p \sqrt{\frac{RT}{2\pi M}} \tag{10}$$

where R_p is the average diameter of the adsorbent, m; D_{eff} is the effective diffusion coefficient, $m^2 \cdot s^{-1}$; ρ_s is the adsorbent packing density, $kg \cdot m^{-3}$; D_{12} is the molecular diffusion coefficient, $m^2 \cdot s^{-1}$; D_{kn} is the component of the Knudsen diffusion coefficient, $m^2 \cdot s^{-1}$; M_1 is the molecular weight of component 1, $kg \cdot mol^{-1}$; M_2 is the molecular weight of component 2, $kg \cdot mol^{-1}$; V_1 is the molar volume of component 1 with the pressure p and temperature T, $m^3 \cdot mol^{-1}$; V_2 for component is the molar volume of component 2 with the pressure p and temperature T, $m^3 \cdot mol^{-1}$; and dp is average micropore diameter of adsorbent, m. Allowing for circuitous phenomenon, D_{12} and D_{kn} are amended to be

$$D'_{12} = \frac{D_{12}}{u_{pdiff}}; D'_{kn} = \frac{D_{kn}}{u_{pkn}}$$

where u_{pdiff} is the molecular diffusion constant and u_{pkn} is the Knudsen molecular diffusion constant.

As a result of the heat and mass transfer coupling, as well as many other factors, it is hard to theoretically calculate the mass transfer coefficient of the LDF model, and the simulation method is most currently used.[10,14,15] This is supported by a large difference among published data in relevant literature. The change of mass transfer coefficients in the desorption process is discussed in this paper.

Model Conditions. Initial conditions:

$$C|_{t=0} = 0 \qquad q|_{t=0} = 0 \qquad T|_{t=0} = T_{0^\circ}$$

Boundary conditions:[16,17]

$$-D_L \left.\frac{\partial C}{\partial z}\right|_{z=0} = u(C|_{z=0^-} - C|_{z=0^+})$$

$$-K_L \left.\frac{\partial T}{\partial z}\right|_{z=0} = \rho_g c_{pg}(T|_{z=0^-} - T|_{z=0^+})$$

$$\left.\frac{\partial C}{\partial z}\right|_{z=L} = 0 \qquad \left.\frac{\partial T}{\partial z}\right|_{z=L} = 0$$

The end conditions of the adsorption are used as the initial conditions of the desorption.

Results and Discussion

Desorption Temperature Changing Conditions. As the desorption absorbs heat, the desorption mass transfer zone temperature decreases. The concentration curve was tested at 20 °C and 105.21 kPa when adsorption occurs with inlet concentrations of (22.60 and 6.14) $g \cdot m^{-3}$ and at different pressures, as shown in Table 2. The measured mass transfer zone temperature changes, and the export concentration curve in the acetone desorption process is shown in Figures 2 and 3.

This shows that vacuum desorption outflow is divided into four characteristic areas: the vacuum concentrated area, fast decay area, the concentration maintenance area (pressure < 60 kPa), and the slow decay area.

The desorption temperatures were set at (15, 20, and 25) °C under a pressure of 105.21 kPa, and adsorption occurred with an import concentration of 6.14 $g \cdot m^{-3}$ under a pressure of

Table 2. Experimental Conditions (I)

serial no.	saturated adsorption weight kg·kg^{-1}	desorption pressure kPa
1	0.24	31.50
2	0.24	53.55
3	0.24	81.90
4	0.24	105.00
5	0.15	31.50
6	0.15	53.55
7	0.15	81.90
8	0.15	105.00

Table 3. Experimental Conditions (II)

serial no.	saturated adsorption weight kg·kg^{-1}	desorption temperature °C
9	0.17	15
10	0.11	25

105.00 kPa. Experimental conditions are shown in Table 3. The measured mass transfer zone temperature changes and the export concentration curve are shown in Figure 3.

The greater the initial concentration of adsorption and the lower the temperature, the greater the amount of saturated adsorption. Figures 2 to 4 show that the greater the amount of saturated adsorption, the larger the temperature difference in the mass transfer zone, but that the temperature drop due to desorption is less than 2 °C.

Impact of Desorption Pressure on the Desorption Penetration Curve. The export concentration curves in Figures 2 and 3 show that when desorption occurs in the saturation adsorption column under different degrees of vacuum, the export concentration changes in two ways: (1) when the desorption vacuum is small (experiment nos. 4, 7, 8), except in the beginning, the acetone concentration at the exit increases because of the vacuum concentration, and the change in concentration is the opposite of that in the adsorption process; namely, it is similar to the situation with an atmospheric pressure purge, which decreases quickly at first and thereafter slowly; and (2) when the desorption vacuum is large (experiment nos. 1, 2, 3 and 5, 6), changes in the concentration are more complicated than those at exports with the atmospheric pressure purge. When the concentration is decreased to a certain degree, there is a period of time when it is maintained or even increased, after which it continues to decline at a slower rate.

The rapid increase of the concentration during the initial desorption of acetone can be explained by the following reasons.

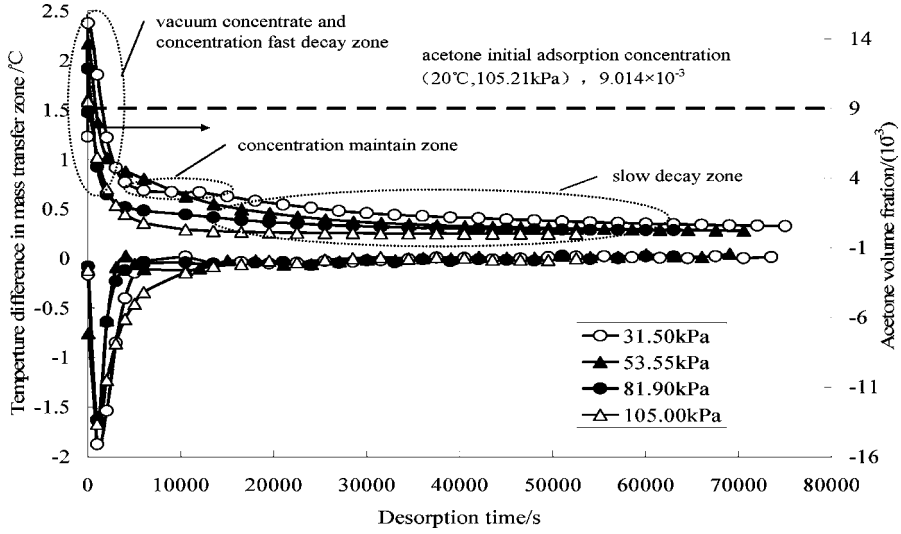

Figure 2. Temperature difference of mass transfer zone and outlet concentration of acetone at different desorption pressures, when the initial concentration of adsorption is 22.60 g·m^{-3}.

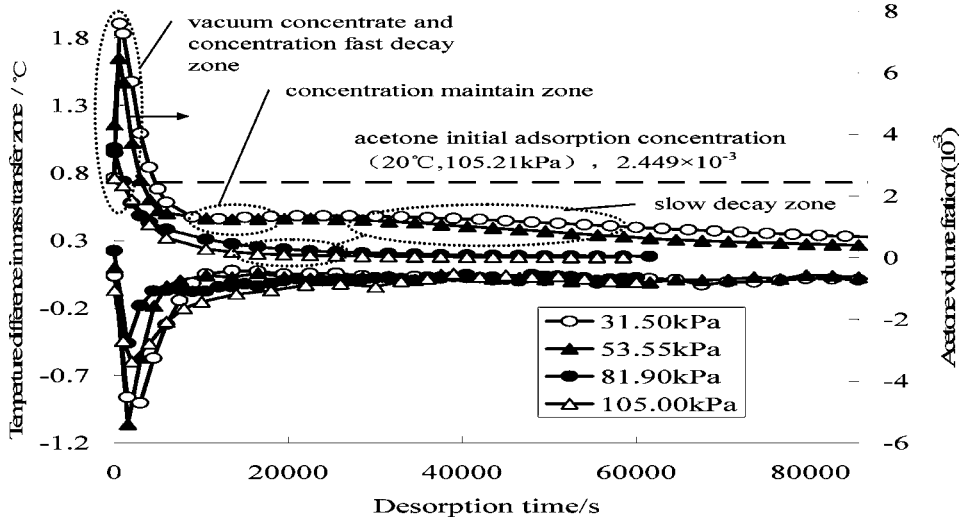

Figure 3. Temperature difference of mass transfer zone and outlet concentration of acetone at different desorption pressures, when the initial concentration of adsorption is 6.14 g·m^{-3}.

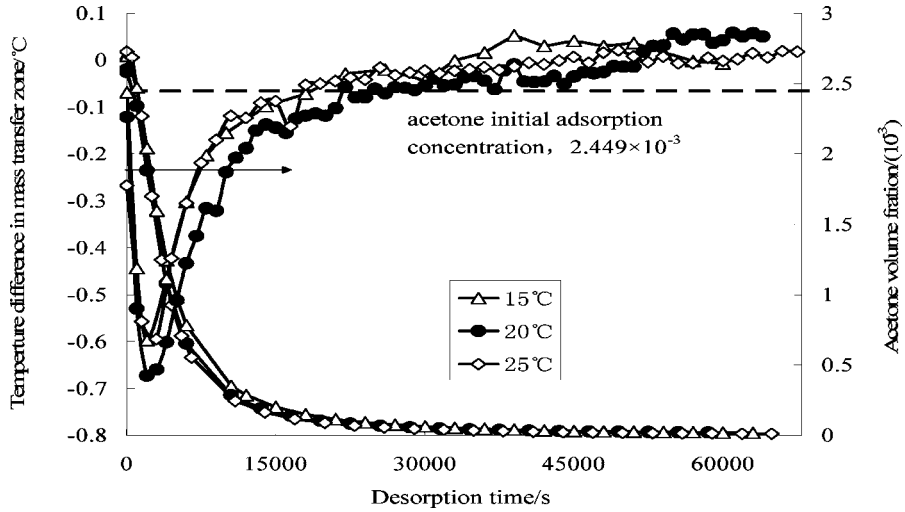

Figure 4. Temperature difference of mass transfer zone and outlet concentration of acetone at different temperatures, when the initial concentration of adsorption is 6.14 g·m^{-3}.

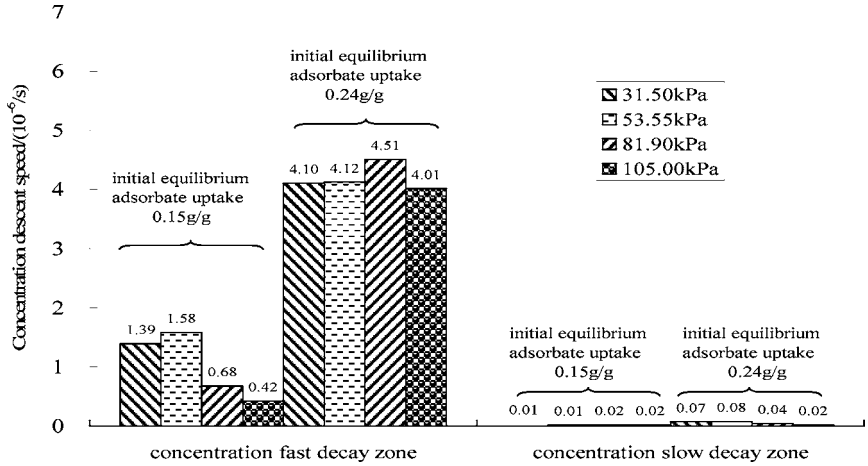

Figure 5. Decrease rate of concentration of different initial concentrations of adsorption and desorption pressure.

Due to evacuation, the total pressure decreases rapidly, and the partial pressure of acetone also decreases and is less than the balance pressure in the beginning of adsorption, to accelerate the acetone desorption from the activated carbon. The volume fraction of acetone in the adsorption column increases rapidly. The greater the desorption vacuum, the higher the degree of increase in the concentration. As the desorption proceeds, the acetone absorbed by activated carbon is gradually reduced, and the export concentration decreases at a rapid rate. Under different desorption pressures, the rates of concentration change in the fast attenuation areas and slowly decaying area and are shown in Figure 5. At the beginning of desorption, there is a large quantity of acetone on the activated carbon, and there is a large difference in the desorption of a gas-phase acetone concentration in the beginning of the corresponding equilibrium adsorption, such that the desorption rate is large when desorption begins. As desorption continues, acetone desorbs continuously from the activated carbon to the gas phase, and the corresponding difference between the relatively small amount of equilibrium adsorption and the desorption rate is low. As shown in Figure 5, the greater the initial adsorption, the greater the slope of the desorption curve and the greater the desorption rate.

In case 2, the maintenance of concentrations may be the result of capillary phenomena.[18] When the pressure is reduced during desorption, the condensed liquid in the large hole evaporates first, and the adsorption film is left on the hole wall. As the pressure decreases further, the condensed liquid in smaller holes evaporates and is left on the hole wall, while the adsorption film becomes thinner on large pore walls, so the amount of desorption caused by reduced pressure consists of two parts: the condensed liquid evaporation corresponding to the pressure change and the decreased thickness of adsorbed film on pore walls. However, because the activated carbon pore size is different, a cavity closed by the condensed liquid may be formed at relatively large pores. As desorption proceeds, the inner cavity pressure is equal to the sum of gas pressure outside the cavity and the condensed liquid pressure, in which the partial pressure of acetone is greater than that outside the cavity. Thus, before the condensed liquid is fully evaporated, the extent of desorption on the inner cavity surface is less than that outside the cavity, and the desorption gas is enclosed in the cavity by condensed fluids. After complete evaporation of the enclosed condensed liquid, this part of the gas is released, so the desorption rate decreases, and the desorption concentration curve is maintained. In Figure 2, when the desorption pressure is less than 81.90 kPa, the acetone export concentration curve shows short-term maintenance, whereas under the conditions shown in Figure 3, there is a smaller trend under the same pressure. This indicates that, under a strong vacuum, the greater the initial adsorption capacity is, the more likely that concentration maintenance occurs, which may be explained by the fact that the greater adsorption concentration, the more holes have capillary cohe-

sion, and the more obvious the effect of molecular vaporization on concentration maintenance.

In addition, Figures 2 and 3 show that the larger degree of vacuum helps to increase the initial concentration of acetone but is not good for the fast desorption of acetone. When the initial adsorption equilibrium capacities are (0.24 and 0.15) $g \cdot g^{-1}$ and the desorption pressures are (31.50, 53.55, 81.90, and 105.00) kPa, the multiples of concentration increase are 1.68, 1.52, 1.31, and 1.06 and 3.0, 2.33, 1.5, and 1.1, respectively. Insert $C_i = py_iM_i/(RT)$ into both sides of eq 6, and calculate the partial derivatives for P and the rate of balance adsorption over pressure.[19] We have $(\partial q^*/\partial p) = (q_{max}RT)/(by_iM_i)p^{-2}$. This shows that the smaller the acetone concentration in evacuation, the greater the rate of balance adsorption over pressure, so the smaller the initial adsorption capacity, the greater the extent of the reduction of the balance adsorption capacity over pressure; in turn, the greater the desorption mass transfer rates, the greater the degree of the increase of the concentration of acetone in the gas phase.

In Figures 2 to 4, the desorption pressure and rates are different; thus, the mass transfer coefficient is different because the pressure affects the diffusion coefficient and absorption capacity, thus affecting the mass transfer coefficient.[8]

Impact of Temperature on Mass Transfer. Figure 4 shows that, under different temperatures, the export concentration curve shape is almost the same, indicating that the mass transfer rate varies slowly with temperature. In Figure 4, the speed of the decline of the acetone concentration did not vary substantially but is the fastest at 25 °C and the slowest at 15 °C. This indicates that the higher the temperature, the greater the rate of acetone desorption, the greater the mass transfer coefficient, and the greater the slope of the desorption curve.

Equations 7, 8, and 9 show that, in addition to the $\partial q/\partial c$ term, the temperature affects the mass transfer coefficient primarily through the D_{eff} term. The temperature difference in the desorption process is less than 2 °C, that is, its range is (0.99 to 1.01). Thus, the D_{12} range is (0.98 to 1.02) $D_{12,o}$, and the D_{kn} range is (0.99 to 1) $D_{kn,o}$. Correspondingly, the largest range of D_{eff} is (0.98 to 1.02) $D_{eff,o}$. The change is less than 2 %, so the temperature has little effect through the improved Langmuir isotherm.[8] We see that the temperature change is less than 2 °C, resulting in a very small difference of $\partial q/\partial c$; therefore, given a little change in temperature, the changes in k and D_{eff} can be ignored.

Discussion on the Impact of Heat and Mass Transfer. Impact of Mass Transfer Coefficient on Desorption Concentration Curve Influenced by Coupling. Equation 7 shows that the mass transfer coefficient depends on $\partial q/\partial c$. As the acetone adsorption on activated carbon can be described by the improved Langmuir isotherm equation,[8] it can be established that, when the gas phase adsorbate concentration is low, $\partial q/\partial c$ is basically constant, and that it is the same as the higher concentration; that is, when the adsorption isotherm is linear, the adsorbate mass transfer coefficient has nothing to do with the concentration.[9] It can be predicted for the acetone desorption process that there are different mass transfer coefficients and diffusion coefficients in different concentrations changing stages.

To explore the impact of coupling heat and mass transfer, numerical simulations were used to discuss the coupling effects of the mass transfer coefficient on the concentration curves of desorption. Table 4 shows some parameters in the desorption mathematical model.

Figure 6 shows the effect of the mass transfer coefficient k on the desorption curve under different degrees of vacuum. As the desorption pressure changes, for the same k, the smaller the pressure, the greater the concentration increases in the vacuum compression zone, and the greater the concentration rate of decrease and the faster the mass transfer. As for the same initial equilibrium adsorption capacity, temperature, and desorption pressure, the greater the k, the greater the mass transfer rate, the steeper the concentration curve, and the sooner the concentration decreases to 0. With the desorption pressure changes, the change in the decreasing rate of concentration due to k changes is not obvious.

Table 4. Primary Parameters in the Model

ε	ε_p	ΔH / kJ·kg^{-1}	R_p / mm
0.428	0.673	620.5	3.16

Figure 7 shows the impact of the change in the mass transfer coefficient k on the desorption concentration curve under different equilibrium adsorption capacities. When the equilibrium adsorption capacity is not the same, for the same k, the greater the equilibrium adsorption capacity, the steeper the concentration curve, the larger the concentration decrease and the faster the mass transfer rate. Figure 7 shows that the change in the rate of decreasing concentration due to k increases as the initial equilibrium adsorption capacity decreases.

Figure 8 shows the impact of the mass transfer coefficient k on the desorption curves under different temperatures. For the same initial equilibrium adsorption capacity, desorption pressure, a 5 °C temperature difference, and k under different temperatures, the concentration curves are almost identical, indicating little sensitivity to temperature.

Figures 6 to 8 show that the impact of the mass transfer coefficient k on concentration is strong at the beginning of

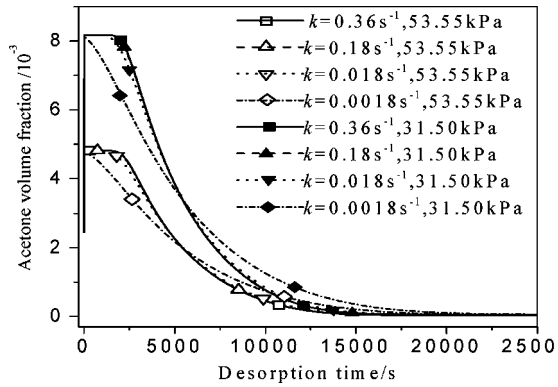

Figure 6. Effects of k on outlet concentration of desorption at different vacuum rates (20 °C, 6.14 $g \cdot m^{-3}$).

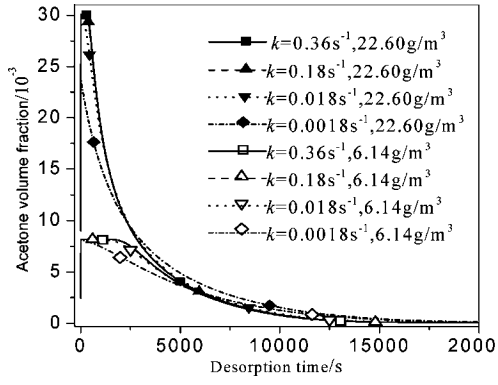

Figure 7. Effects of k on the outlet concentration of desorption with different saturation adsorption quantities (20 °C, 31.50 kPa).

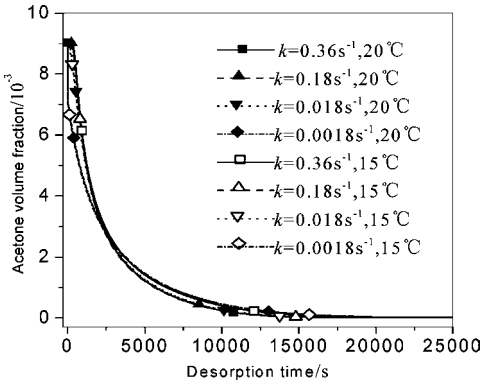

Figure 8. Effects of k on the outlet concentration of desorption at different temperatures (105.00 kPa, 22.60 g·m^{-3}).

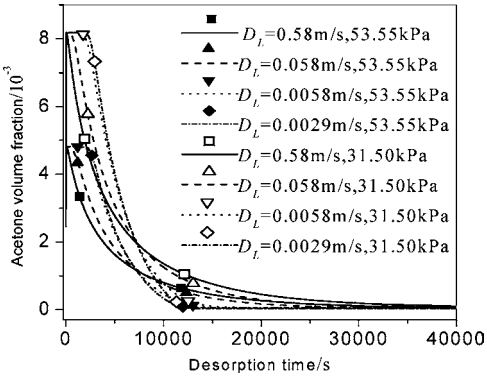

Figure 9. Effects of D_L on outlet concentration of desorption at different vacuum rates (20 °C, 6.14 g·m^{-3}).

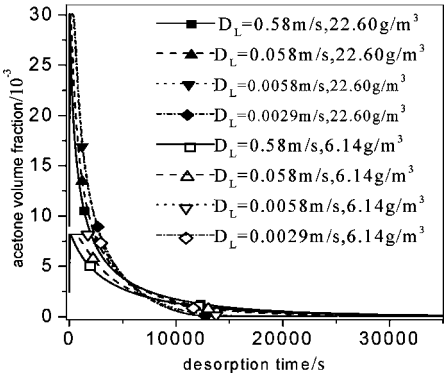

Figure 10. Effects of D_L on outlet concentration of desorption with different saturation adsorption quantities (20 °C, 31.50 kPa).

desorption, but that this subsequently decreases, especially in the slowly decaying areas.

Figure 9 shows the impact of the axial diffusion coefficient D_L on the desorption concentration curves. For the same initial equilibrium adsorption capacity, temperature, and desorption pressures, the greater the D_L, the smaller the mass transfer rate, the flatter the concentration curve, and the later the concentration is reduced to 0. The change in the decreasing concentration rate due to the D_L value increases as the desorption decreases; when the pressure is low, the diffusion is more obvious.

Figure 10 shows the impact of D_L on concentration under different equilibrium adsorption capacities. The rate of decreasing concentration due to decreasing D_L decreases as the equilibrium adsorption capacity increases. For different temperatures, the impact of D_L on the desorption curves is shown in Figure 11. For the same initial equilibrium adsorption capacity, desorption pressure, and a 5 °C temperature difference,

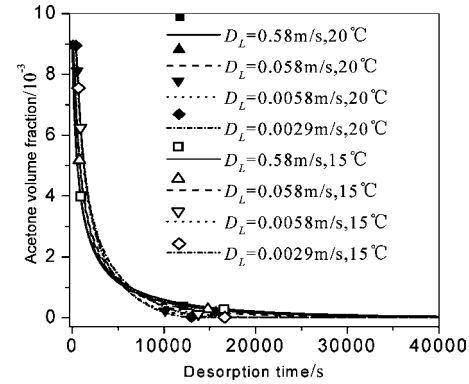

Figure 11. Effects of D_L on outlet concentration of desorption at different temperatures (105.00 kPa, 22.60 g·m^{-3}).

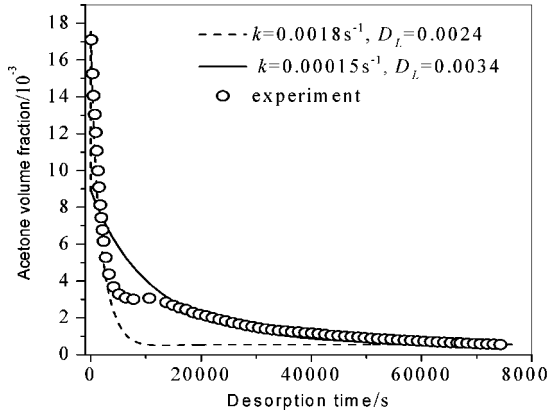

Figure 12. Simulation results of experiment 1 with constant k and D_L.

in the first half of the concentration curve, the smaller the D_L value is, the higher the concentration, and the concentration does not change with temperature; in the second half of the concentration curve, for the same D_L value, the lower the temperature, the higher the concentration. The effect of reducing D_L on the concentration increase is more obvious at lower temperatures.

Comparing Figures 6 to 11, the impact of concentration changes when the D_L changes by a factor of 100, which is bigger than the change of the k value on the concentration curves. The impact of D_L changing is not only in the initial desorption, but the decrease of D_L also causes the concentration to increase in the slow decay area, which is contrary to the adsorption situation.[2]

The export acetone concentration decline rate on activated carbon is very different before and after the maintenance phase, with the maintenance emergence time as the subpoint. Figure 12 shows the experimental simulations of the no. 1 experiment when the mass transfer coefficient and axial dispersion coefficient are given certain values. The simulated curves with various k and D_L values are very different than that when the concentration is constant. If the simulation results coincide with those in the vacuum compression area and the rapid concentration decay area, it is difficult to demonstrate coincidence with the slow decay zone data, and vice versa. This shows that, under large vacuums and concentration maintenance areas, the calculation with fixed values of k and D_L can hardly correspond well to the experimental data in the entire desorption process.

In short, the simulation concentration curve shows a law for the impact of coupling mass transfer coefficients on the desorption curves: in vacuum desorption, when the desorption vacuum is small, the mass transfer coefficient and diffusion

Table 5. k and D_L in the Simulation

	k (s^{-1})		D_L ($m \cdot s^{-1}$)	
serial no.	vacuum concentration and rapidly decay zone	concentration slowly decay zone	vacuum concentration and rapidly decay zone	concentration slowly decay zone
1	0.0018	0.00025	0.0024	0.00074
2	0.0034	0.0005	0.0026	0.0034
3	0.038	0.00035	0.0028	0.0074
5	0.0019	0.0015	0.0094	0.0074
6	0.008	0.00085	0.035	0.0064
4	0.18		0.0058	
7	0.038		0.95	
8	0.6		0.055	
9	0.6		0.050	
10	0.6		0.065	

coefficient are almost unchanged. However, as the vacuum degree decreases, in particular, when it is lower than 50 kPa, the mass transfer coefficient and diffusion coefficient may change, and the mass transfer coefficient and diffusion coefficient have different characteristics. This also indicates that, after capillary phenomena take place, the mass transfer coefficient is influenced by the desorption pressure and decreases with desorption pressure reduction; desorption temperature fluctuations have little effect on the mass transfer coefficient. It is also consistent with the previous theoretical analysis, such that it can be concluded that the mass transfer coefficient is different at different desorption stages. Simulation serves as a way to obtain data that is hard to obtain in micropoles.

Mass Transfer Coefficient at Different Desorption Stages with the Coupled Effect. On the basis of the theoretical analysis and simulation discussion, for a constant concentration, it is necessary to find the mass transfer coefficient and axial dispersion coefficient in different stages, with the emergence time as the subpoints, before and after which different mass transfer coefficients and axial dispersion coefficients are obtained. For the situations without concentration maintenance, good results with fixed k and D_L values were found. In experiments 1 to 10, the export concentration curves are shown in Figure 13 to 15.

k and D_L values in the simulation of experimental data are shown in Table 5. This shows that the model can be used to simulate the desorption of acetone from activated carbon. The average error between the experiment and simulation is less than 10 %.

Because the LDF mass transfer coefficient is greatly impacted by the saturated absorption capacity, the saturated absorption capacity is determined by the partial pressure of acetone rather than the volume percentage. In the experiment, the order of partial pressure of acetone is experiment 4 > experiment 3 > experiment 2 > experiment 1, and in the other group, experiment 8 > experiment 7 > experiment 6 > experiment 5. Table 4 shows that the LDF mass transfer coefficient increases as the partial pressure of acetone increases. Experiments 8, 9, and 10 simulation experiments have the same mass transfer coefficient, which indicates that there is no big change in the mass transfer coefficient under a 10 °C temperature difference.

The simulating calculation shows that, in contrast to adsorption, the axial dispersion coefficient D_L is much bigger for desorption in this experiment and should not be ignored. This indicates that free diffusion and microporous molecular Knudsen proliferation in the desorption process have a greater role than in adsorption. In the D_L subvalues, it is found that the difference between D_L values in two stages is far less than the differences in the k values, but that the impact of temperature on D_L is much bigger than that on the k value: it increases as temperature rises. This is because both the free molecular diffusion and Knudsen diffusion increase as the temperature increases.

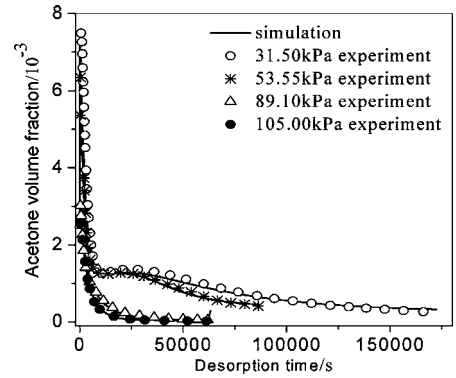

Figure 14. Simulation of outlet concentration in experiments 5 to 8.

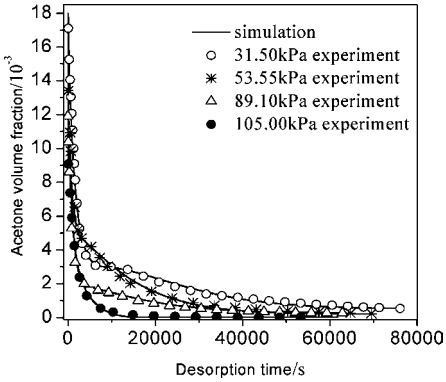

Figure 13. Simulation of outlet concentration in experiments 1 to 4.

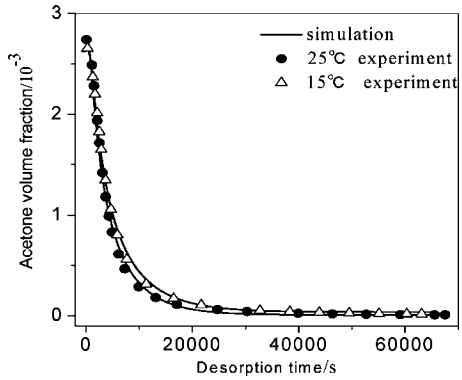

Figure 15. Simulation of outlet concentration in experiments 9 and 10.

Conclusions

In this paper, on the basis of the fixed-bed vacuum desorption process, the mass balance, mass transfer process, and energy conservation model are established, and for the models used for the performance calculation under different experimental conditions, the simulated results agree well with the experimental results. Thus, the model can be used for the prediction of some factors to be determined. The following conclusions can be drawn by numerical simulations.

(1) The desorption concentration curve can be divided into a vacuum concentration area, rapid attenuation area, and slowly decaying area: when the desorption pressure is 31.5 kPa, the desorption export concentrations which are 6.14 $g \cdot m^{-3}$ and 22.60 $g \cdot m^{-3}$ go through a long period of rebounds and holds before slowly declining, and when the desorption pressure is 53.55 kPa, only the initial concentration of adsorption of 6.14 $g \cdot m^{-3}$ has this trend.

(2) In the vacuum desorption process, the mass transfer coefficient and diffusion coefficient do not change substantially when the desorption vacuum degree is small. However, as the vacuum degree decreases, in particular, when it is lower than 50 kPa, the mass transfer coefficient and diffusion coefficient change and have different characteristics. In particular, the capillary phenomena in the production after the mass transfer coefficient by the desorption pressure decrease with the desorption pressure to reduce the trend. This also indicates that after capillary phenomena take place, the mass transfer coefficient is influenced by the desorption pressure and decreases with desorption pressure reduction.

(3) It is found from experimental and theoretical analysis that, when the temperature is from (15 to 25) °C, if the temperature changes caused by desorption are not big, the mass transfer coefficient change is not great.

(4) If the adsorption isotherm lines have linear relations, the concentration has little effect on the mass transfer coefficient.

(5) Simulating the mass transfer coefficient and axial dispersion coefficient phase by phase can meet the experimental data well, serving as a good way to acquire the data, which is hard to obtain in micropoles.

(6) The axial diffusion coefficient D_L has a large value in the experimental conditions and should not be ignored. The temperature has a greater impact on k than D_L.

Literature Cited

(1) Delgada, J. A.; Rodrigues, A. E. Analysis of the boundary conditions for the simulation of the pressure equalization step in PSA cycles. *Chem. Eng. Sci.* **2008**, *63*, 4452–4463.

(2) Subebach, W. D. *Druckwechsel adsorption von organischen dämpfen*; Ruhr-Universitaet Bochum: Bochum, Germany, 2002.

(3) Wilde, D. J.; Marin, G. B. Investigation of simultaneous adsorption of SO_2 and NO_X on Na-γ-alumina with transient techniques. *Catal. Today* **2000**, *62*, 319–328.

(4) Ren, J.; Zhou, J.; Luo, Z. Fix-bed experiments and mathematical modeling for adsorption of mercury vapors. *Proc. CSEE* **2006**, *26*, 1–6.

(5) Kozo, M.; Hisaji, M.; Naoki, Y. Multi-component behavior of fixed-bed adsorption of dioxins by activated carbon fiber. *Chemosphere* **2005**, *61*, 941–946.

(6) Jun, Z.; Paul, A. W.; Xiao, P. Effect of process parameters on power requirements of vacuum swing adsorption technology for CO_2 capture from flue gas. *Energy Convers. Manage.* **2008**, *49*, 346–356.

(7) Budner, Z.; Dula, J.; Podstawa, W. Study and modeling of the vacuum swing adsorption(VSA) process employed in the production of oxygen. *Trans. Inst. Chem. Eng.* **1999**, *77*, 405–412.

(8) Liqing, L. *Theoretical and experimental study on the treatment of organic vapors by adsorption and pressure swing adsorption (PSA)*; Hunan University: Changsha, China, 2004.

(9) Kast, W. *Adsorption aus der gasphase*; Weinheim Verlag: Berlin, Germany, 1988.

(10) Leinekugel-le-Cocq, D.; Tayakout-Fayolle, M.; Gorrec, Y. L.; Christian, J. A double linear driving force approximation for non-isothermal mass transfer modeling through bi-disperse adsorbents. *Chem. Eng. Sci.* **2007**, *62*, 4040–4053.

(11) Hwang, K. S.; Jun, J. H.; Lee, W. K. Fixed-bed adsorption for bulk component system, non-equilibrium, non-isothermal and non-adiabatic model. *Chem. Eng. Sci.* **1995**, *50*, 813–825.

(12) Li, L.; Zhu, Z.; Qin, Y. Simulation on isotherm adsorption of two-component organic gas and heat and mass transfer analysis. *Proc. CSEE* **2008**, *28*, 16–52.

(13) Ruthven, D. M. *Principles of adsorption and adsorption process*; John Wiley and Sons: New York, 1984.

(14) Sircar, S. Gas sorption kinetics by differential closed-loop recycle method: Effect of heat of adsorption. *Adsorption* **2006**, *12*, 259–266.

(15) Sircar, S.; Hufton, J. R. Why Does the linear driving force model for adsorption kinetics work. *Adsorption* **2000**, *6*, 137–147.

(16) Nastai, J. F.; Ambrozek, B.; Rundick, J. Simulation studies of vacuum and temperature swing adsorption process for the removal of VOC from waste air streams. *Int. Commun. Heat Mass Transfer* **2006**, *33*, 80–86.

(17) Sankarrao, B.; Gupta, S. K. Modeling and simulation of fixed bed adsorbers (FBAs) for multi-component gaseous separations. *Comput. Chem. Eng.* **2007**, *31*, 1282–1295.

(18) Song, L.; Sun, Z.; Duan, L.; Gui, J. Adsorption and diffusion properties of hydrocarbons in zeolites. *Microporous Mesoporous Mater.* **2007**, *104*, 115–128.

(19) Lee, S. W.; Park, H. J.; Lee, M. G. Comparison of adsorption characteristics according to polarity difference of acetone vapor and toluene vapor on silica-alumina fixed-bed reactor. *Ind. Eng. Chem.* **2008**, *14*, 10–17.

Received for review April 12, 2010. Accepted August 28, 2010. This work was funded by the National Natural Science Foundation of China (No. 20679154 and No. 20976200).

JE1003548